Detection and Analysis of Marine Green Algae Based on Artificial Intelligence

Le Gao, Xiaofeng Li, Yuan Guo, Fanzhou Kong, and Rencheng Yu

1 Introduction

Harmful algal blooms (HAB), e.g., Yellow sea green algae, are disastrous ecological events in coastal oceans. During the blooming period, the rapid biomass increase severely impacts the coastal ecosystems and even the Olympic regatta games in 2008 [6, 13–15, 17, 20, 22, 23].

Satellite remote sensing is a suitable means for green algae (*U. prolifera*) observation and analysis because of the frequent data acquisition and broad coverage area [5, 7]. Existing studies mostly use passive optical-sensor images of 250-1,000 m resolution., e.g., Moderate Resolution Imaging Spectroradiometer (MODIS). The floating *U. prolifera* modulate the ocean color properties to make sea surface appear the prominent algae features in optical images [2, 8, 10, 21]. Active Synthetic aperture radar (SAR) images provide sea surface roughness with a resolution of tens of meters. The floating algae on the sea surface behave like a volume-scattering hard object, and the algae patch area's reflected signal is much stronger than that backscattered one from the surrounding water, which appears as brighter regions in SAR images. SAR has become another option for detecting algae because some SAR images have become free and open, e.g., the European Space Agency (ESA) Sentinel-1 and Chinese Gaofen-3 data. For optical-sensor images, biological index methods, e.g., NDVI (Normalized Difference Vegetation Index) and FAI (Floating Algae Index), are commonly used [1, 5]. For SAR-sensor images, previous studies usually use grey, roughness or backscatter coefficient difference to identify the target [4, 12]. However, these methods cannot effectively fuse the information from the optical and SAR images since the physical mechanisms of optical- and SAR-sensors for *U. prolifera* detection are very different. Based on the algae's characteristics in the two sensors' images, deep-learning (DL) offers a possibility to perform data fusion

L. Gao · X. Li (✉) · Y. Guo
CAS Key Laboratory of Ocean Circulation and Waves, Institute of Oceanology, Chinese Academy of Sciences, Qingdao 266071, China
e-mail: lixf@qdio.ac.cn

F. Kong · R. Yu
Key Laboratory of Marine Ecology and Environmental Sciences, Institute of Oceanology, Chinese Academy of Sciences, Qingdao 266071, China

X. Li and F. Wang (eds.), *Artificial Intelligence Oceanography*,
https://doi.org/10.1007/978-981-19-6375-9_13

[12]. *U. prolifera* algae have the thalli's hollow tubular structure. During its blooms, some parts of the algae body are exposed above the sea surface, while other parts are submerged below the surface. An optical sensor can collect spectral information at a certain sea depth to effectively capture the floating and underwater part of the algae [7, 11]. The SAR sensor captures only the floating part on the sea surface. Thus, we can define the floating and submerged algae ratio (FS ratio), i.e., part of SAR-sensor detection/part of optical-sensor detection. The objectives of this research include 1) proposing a DL network to detect *U. prolifera* from optical and SAR images better, and 2) using the defined FS ratio to represent algae life stages.

2 Data and Methodology

2.1 Satellite Images and Labels

We collected geometrically and radiometrically corrected 250 m spatial resolution MODIS true-color imagery (Bands: 1/4/3) containing algae patches in the Yellow Sea, and these MODIS images are under clear sky conditions from 2008 to 2021. Compared to the surrounding seawater, the *U. prolifera* algae show more prominent green slick/patch features (Fig. 1a–d). Using the Labelme software [16], we can label sample image slices containing different algae shapes for DL algorithm development. Finally, 1,055 pairs of MODIS labelled samples were obtained, and 680/292/83 pairs were used as training/validation/testing sets.

We also collected Sentinel-1 Level-1 GRD (Ground Range Detected) dual-polarization (VV, VH) interferometric wide images with 10 m spatial resolution and 250 km swath and the Chinese GaoFen-3 SAR Fine Stripe Mode II (FSII) dual-polarization (HH, HV) image with 10 m resolution and 100 km swath between 2015 and 2019. All SAR images were processed with speckle filtering and geometric, radiometric, orthometric, and terrain corrections to improve image quality using the Sentinel Application Platform (SNAP) 7.0 software. The algae patches show bright spots/slicks in SAR images (Fig. 1e). We marked 4,071 pairs of the algae labelled samples; 2,086/895/1,090 pairs were used as training/validation/testing sets.

2.2 UNet-Based Algae Detection Network (AlgaeNet)

We propose a DL-based model, AlgaeNet, to detect the algae patches better. Figure 2 shows the model's system diagram based on the U-Net framework [12, 16]. Optical and SAR images are input to the DL model separately,and the corresponding detection result of the optical (SAR) image is Algae coverage-1 (2) through the improved model. Then the model can perform data fusion based on the two sensors' detection results, and the FS ratio can be estimated by Algae coverage-2/Algae coverage-1.

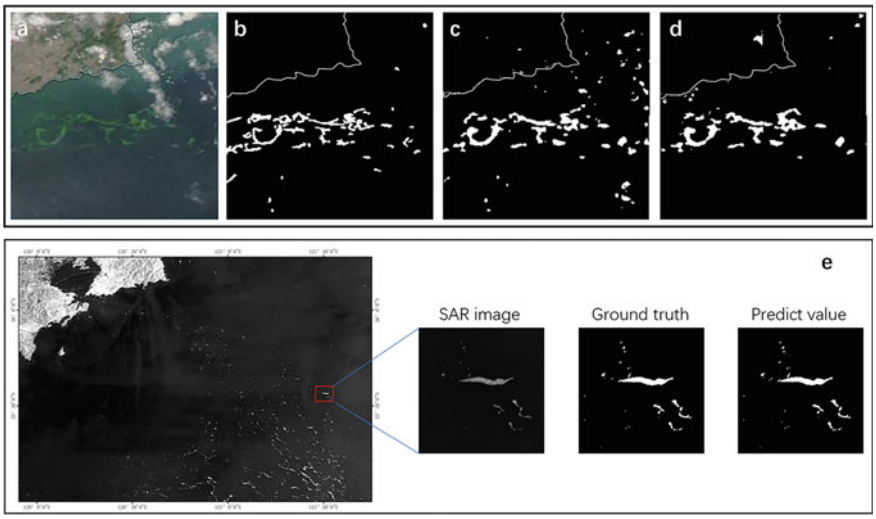

Fig. 1 U. prolifera algae blooms in Yellow sea and algae detection examples at the pixel level in green tide bloom period. **a** the random selected MODIS true-color images on June 25, 2008; **b** is the marked ground truth by manual; **c** is the predicted value of the classic U-Net model; **d** is the corresponding predicted value of the AlgaeNet model; the white dots are algae pixels, and the black are the background ocean; **e** is an algae detection example based on the AlgaeNet model in Sentinel-1 SAR images

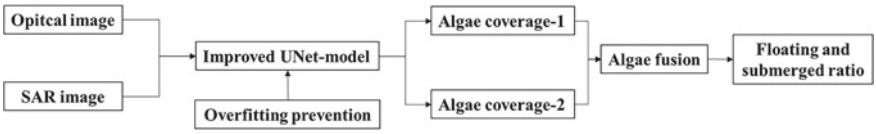

Fig. 2 AlgaeNet model design. Algae coverage-1 (2) is based on MODIS (SAR) images

During the DL architecture design, we should pay particular attention to maintaining the tradeoff between optimization and generalization of the network. The overfitting of the algae detection model is usually prevented mainly through the following three methods: dropout, weight regularization, and batch normalization. We found that batch normalization (BN) and weight regularization were beneficial for the network of the three technologies. BN provided any layer with zero mean/unit variance in the DL model [9]. The initialization type of weights could cause a digression to gradients, meaning the gradients have to compensate for the outliers. BN regularizes the gradient by normalizing activations throughout the network. It prevents small parameter changes from amplifying into more significant and suboptimal changes in gradients' activations. L2 weight regularization is also added to each hidden layer. During optimization, L2 regularization adds penalty items to model parameters or activation values in the hidden layer, limiting the model parameters too much/too large to avoid the network being too complicated. These penalty terms will be used as the network's ultimate optimization goal.

Table 1 Performance of AlgaeNet model

Input data	AI-Model	Output (%)				
		Accuracy	Precision	Recall	F1 score	IoU
MODIS	Classic U-Net	96.37	62.96	53.84	58.04	37.89
	AlgaeNet	97.51	66.61	55.41	60.50	42.62
Sentinel-1/GF-3 SAR		99.83	95.35	92.04	93.67	88.09
	Random Forest	99.39	72.95	87.96	79.96	66.60

2.3 Model's Performance

The performance evaluation of the AlgaeNet model includes the assessments of the algae detection performance for MODIS and SAR images, respectively. For evaluating the AlgaeNet-MODIS model, Table I shows that the performance of the AlgaeNet-MODIS model is better than the original U-Net model; the AlgaeNet-MODIS (U-Net) model reached 97.51 (96.37)%, 66.61 (62.96)%, 55.41 (53.84)%, 60.50 (58.04)%, and 42.62 (37.89)% in the five commonly used indicators of Accuracy, Precision, Recall, F1_Score, and Mean Intersection over Union (IoU). For the evaluation of AlgaeNet-SAR, the model reached 99.83, 95.35, 92.04, 93.67, and 88.09% in the five indicators, which are significantly better than AlgaeNet-MODIS. Figure 1 also gives a visual presentation of the algae detection performance in the *U. prolifera* blooming period. Finally, we compared the model's further with the recent neural networks: Random Forest (RF) models. Table 1 shows that our model has significantly higher performance than the RF model and indicates the excellent portability of the particular improvement strategy in the networks.

3 Results and Discussion

The AlgaeNet model was used in MODIS and SAR images to examine the algae coverage changes in 2020 and 2021. Figure 3 shows that the maximum biological coverage in 2021 is nearly four times that of 2020. This significant difference has attracted widespread attention, and it is related to nutrients, sea surface temperature, sea surface salinity, seaweed planting valve area and valve frame recovery time, species competition, etc. [3, 18, 21].

We used the AlgaeNet model to process the collected MODIS and SAR images and acquired twelve pairs of spatiotemporally matching MODIS and SAR images/slicks. Figure 4 shows that the algae patches captured by MODIS and SAR sensors have a highly consistent spatial distribution pattern (Fig. 4b-c). In addition, we also found one interesting detail: for the big algae patches/slicks with a high aggregation degree,

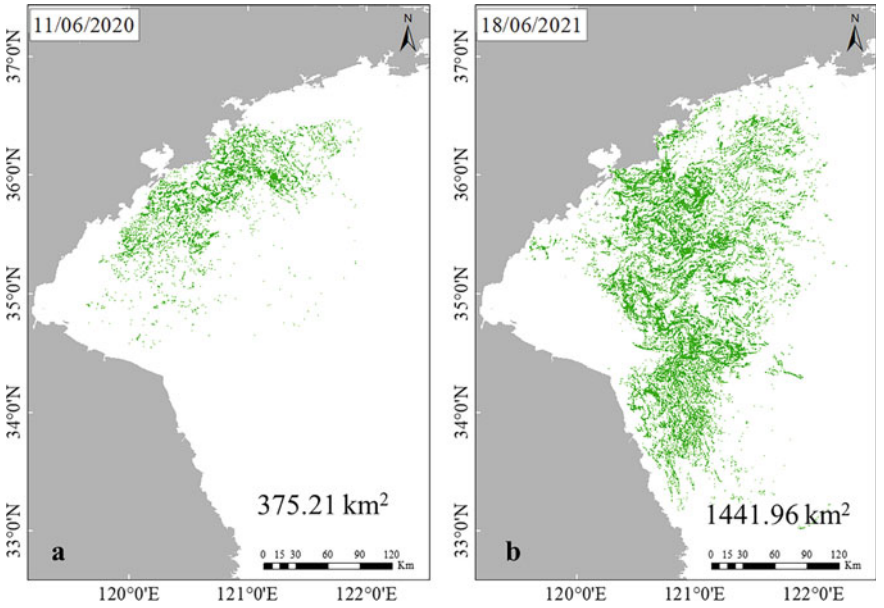

Fig. 3 The detected maximum algae coverage in 2020 **a** and 2021 **b** in Yellow Sea

the margin of the algae patches observed by the MODIS sensor is broader than that observed by the SAR sensor. That is due to the unique floating mechanism of the algae body. The *U. prolifera* algae has the thalli's hollow tubular structure and floats on the sea surface; some parts of the algae body are exposed above the sea surface, while others are submerged below the surface. Therefore, optical sensors can collect spectral information at a certain sea depth to effectively capture the underwater part of the algae [7, 11]. On the other hand, the SAR sensors capture only the floating part on the sea surface. Thus, we can estimate the floating and submerged algae ratio (FS ratio) of *U. prolifera* algae.

As shown in Fig. 5, the FS ratio reflects the changes in the floating status of U.prolifera. Based on the algae distribution, coverage, and biomass results of the collected MODIS and SAR images from 2008-2021/2015-2019, the *U. prolifera* bloom originated from the Subei Shoal and drifted northward experienced different phases from initiation, development, maintenance, and decline. At the various stages of the *U. prolifera* bloom, the floating *U. prolifera* underwent morphological changes. At the initiation phase in the Subei Shoal, the *U. prolifera* algae had a large proportion submerged in seawater [19] and rare algae biomass. Based on the two matching MODIS AND SAR image pairs, the FS ratio of the algae body was less than 5% (Fig. 4). During the development phase, the biomass of *U. prolifera* rapidly increased. A large proportion of *U. prolifera* became floating due to the optimal illumination and temperature, and therefore FS ratio quickly increased to 24.75%, and some local areas even reached more than 40%. During the maintenance phase of the *U.*

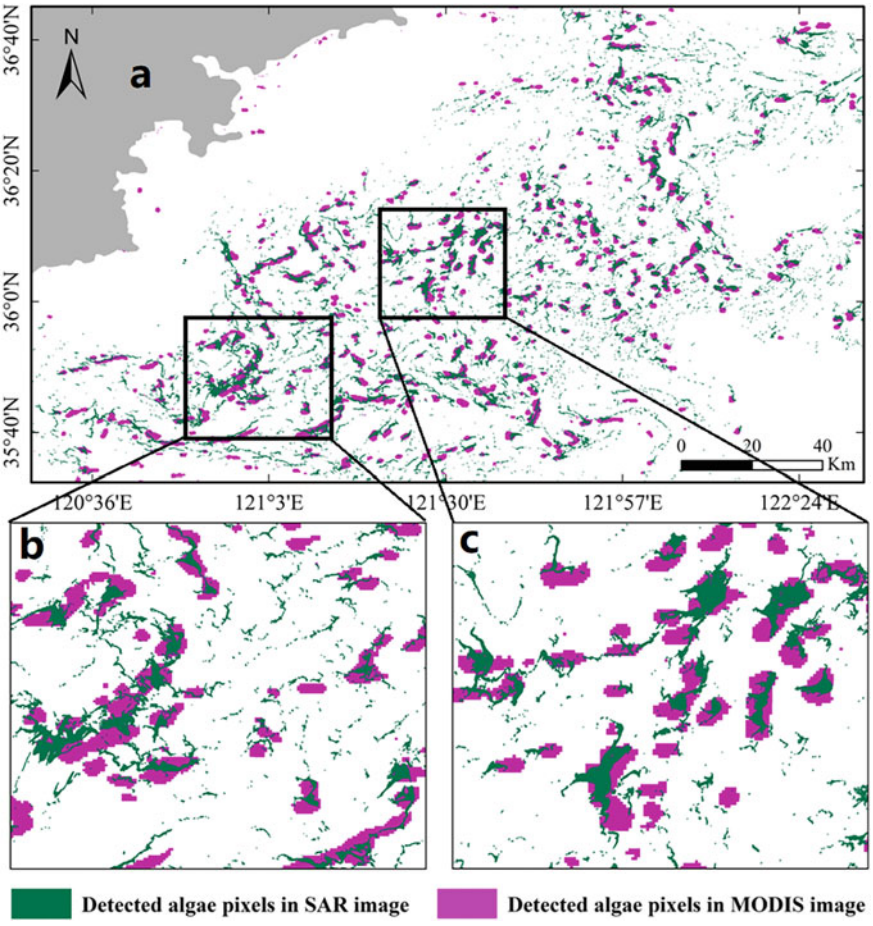

Fig. 4 Algae FS ratio estimation. **a** detected algae pixels between MODIS and SAR images; **b** and **c** corresponds to the enlarged view of two randomly selected sub-areas

prolifera bloom, the *U. prolifera* algae moved northward, and the biomass and FS ratio remained at a high level, basically unchanged, shown as the dotted box of ~21.35%. During the decline phase of the bloom, there were almost no algae near Subei Shoal, and the FS ratio of algae patches in the Yellow Sea decreased rapidly to 14.33%. Therefore, in the entire life phase, the FS ratio of the *U. prolifera* had a parabolic process from increasing, maintaining, and then decreasing. The rates of increasing (initiation phase) and decreasing (decline phase) were high-speed compared to the development and maintenance phases.

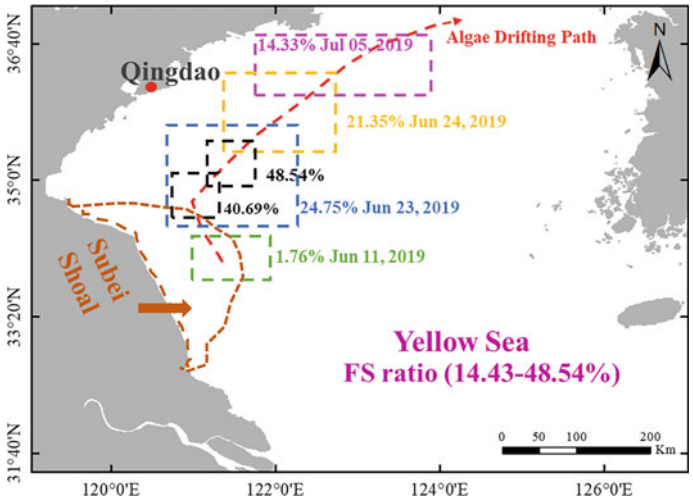

Fig. 5 FS ratio: a life status indicator of *U. prolifera* algae

4 Conclusions

This chapter establishes an improved DL model for detecting *U. prolifera* algae in MODIS and SAR images, and the model has a high detection accuracy, i.e., 97.51%, and Mean IoU to 42.62% for MODIS images and 99.83% and 88.09% for SAR images. The detection results show that the maximum biological coverage in 2021 is almost four times that of 2020 due to various natural and manufactured reasons. Besides, we can take the FS ratio as an excellent indicator to reflect the life status of floating *U. prolifera* algae.

References

1. Blondeau-Patissier D, Gower JF, Dekker AG, Phinn SR, Brando VE (2014) A review of ocean color remote sensing methods and statistical techniques for the detection, mapping and analysis of phytoplankton blooms in coastal and open oceans. Progress Oceanogr 123:123–144
2. Cao Y, Wu Y, Fang Z, Cui X, Liang J, Song X (2019) Spatiotemporal patterns and morphological characteristics of Ulva prolifera distribution in the Yellow Sea, China in 2016–2018. Remote Sens 11(4):445
3. Fan S, Fu M, Wang Z, Zhang X, Song W, Li Y, Liu G, Shi X, Wang X, Zhu M (2015) Temporal variation of green macroalgal assemblage on porphyra aquaculture rafts in the Subei Shoal, China. Estuar Coast Shelf Sci 163:23–28
4. Geng X, Li P, Yang J, Shi L, Li Xm, Zhao J (2020) Ulva prolifera detection with dual-polarization GF-3 SAR data. In: IOP conference series: earth and environmental science, vol 502, p 012026. IOP Publishing
5. Hu C (2009) A novel ocean color index to detect floating algae in the global oceans. Remote Sens Environ 113(10):2118–2129

6. Hu C, Li D, Chen C, Ge J, Muller-Karger FE, Liu J, Yu F, He MX (2010) On the recurrent Ulva prolifera blooms in the Yellow Sea and East China Sea. J Geophys Res: Oceans 115(C5)
7. Hu C, Feng L, Hardy RF, Hochberg EJ (2015) Spectral and spatial requirements of remote measurements of pelagic sargassum macroalgae. Remote Sens Environ 167:229–246
8. Hu L, Zeng K, Hu C, He MX (2019) On the remote estimation of Ulva prolifera areal coverage and biomass. Remote Sens Environ 223:194–207
9. Ioffe S, Szegedy C (2015) Batch normalization: Accelerating deep network training by reducing internal covariate shift. In: International conference on machine learning, PMLR, pp 448–456
10. Lee JH, Pang IC, Moon IJ, Ryu JH (2011) On physical factors that controlled the massive green tide occurrence along the southern coast of the Shandong Peninsula in 2008: a numerical study using a particle-tracking experiment. J Geophys Res: Oceans 116(C12)
11. Lee ZP, Du KP, Arnone R (2005) A model for the diffuse attenuation coefficient of downwelling irradiance. J Geophys Res: Oceans 110(C2)
12. Li X, Liu B, Zheng G, Ren Y, Zhang S, Liu Y, Gao L, Liu Y, Zhang B, Wang F (2020) Deep-learning-based information mining from ocean remote-sensing imagery. Nat Sci Rev 7(10):1584–1605
13. Liu D, Keesing JK, He P, Wang Z, Shi Y, Wang Y (2013a) The world's largest macroalgal bloom in the Yellow Sea, China: formation and implications. Estuar Coast Shelf Sci 129:2–10
14. Liu F, Pang S, Chopin T, Gao S, Shan T, Zhao X, Li J (2013b) Understanding the recurrent large-scale green tide in the Yellow Sea: temporal and spatial correlations between multiple geographical, aquacultural and biological factors. Marine Environ Res 83:38–47
15. Lü X, Qiao F (2008) Distribution of sunken macroalgae against the background of tidal circulation in the coastal waters of Qingdao, China, in summer 2008. Geophys Res Lett 35(23)
16. Ronneberger O, Fischer P, Brox T (2015) U-Net: Convolutional networks for biomedical image segmentation. In: International conference on medical image computing and computer-assisted intervention, pp 234–241. Springer
17. Smetacek V, Zingone A (2013) Green and golden seaweed tides on the rise. Nature 504(7478):84–88
18. Song W, Peng K, Xiao J, Li Y, Wang Z, Liu X, Fu M, Fan S, Zhu M, Li R (2015) Effects of temperature on the germination of green algae micro-propagules in coastal waters of the Subei Shoal, China. Estuar Coast Shelf Sci 163:63–68
19. Xiao J, Fan S, Wang Z, Fu M, Song H, Wang X, Yuan C, Pang M, Miao X, Zhang X (2020) Decadal characteristics of the floating Ulva and sargassum in the Subei Shoal. Yellow Sea. Acta Oceanologica Sinica 39(10):1–10
20. Xiao X, Agusti S, Lin F, Li K, Pan Y, Yu Y, Zheng Y, Wu J, Duarte CM (2017) Nutrient removal from Chinese coastal waters by large-scale seaweed aquaculture. Sci Rep 7(1):1–6
21. Xing Q, An D, Zheng X, Wei Z, Wang X, Li L, Tian L, Chen J (2019) Monitoring seaweed aquaculture in the Yellow Sea with multiple sensors for managing the disaster of macroalgal blooms. Remote Sens Environ 231:111279
22. Zhang J, Zhao P, Huo Y, Yu K, He P (2017) The fast expansion of Pyropia aquaculture in "Sansha" regions should be mainly responsible for the Ulva blooms in Yellow Sea. Estuar Coast Shelf Sci 189:58–65
23. Zhang Y, He P, Li H, Li G, Liu J, Jiao F, Zhang J, Huo Y, Shi X, Su R et al (2019) Ulva prolifera green-tide outbreaks and their environmental impact in the Yellow Sea. China, National Science Review